



HAL
open science

Two distinct binding sites for high potential iron-sulfur protein and cytochrome c on the reaction center-bound cytochrome of *Rubrivivax gelatinosus*

Jean Alric, Makoto Yoshida, Kenji V P Nagashima, Rainer Hienerwadel, Pierre Parot, André Verméglio, Shu-Wen W Chen, Jean-Luc Pellequer

► To cite this version:

Jean Alric, Makoto Yoshida, Kenji V P Nagashima, Rainer Hienerwadel, Pierre Parot, et al.. Two distinct binding sites for high potential iron-sulfur protein and cytochrome c on the reaction center-bound cytochrome of *Rubrivivax gelatinosus*. *Journal of Biological Chemistry*, 2004, 279, pp.32545 - 32553. 10.1074/jbc.m401784200 . hal-03562041

HAL Id: hal-03562041

<https://hal.science/hal-03562041>

Submitted on 8 Feb 2022

HAL is a multi-disciplinary open access archive for the deposit and dissemination of scientific research documents, whether they are published or not. The documents may come from teaching and research institutions in France or abroad, or from public or private research centers.

L'archive ouverte pluridisciplinaire **HAL**, est destinée au dépôt et à la diffusion de documents scientifiques de niveau recherche, publiés ou non, émanant des établissements d'enseignement et de recherche français ou étrangers, des laboratoires publics ou privés.

Two Distinct Binding Sites for High Potential Iron-Sulfur Protein and Cytochrome *c* on the Reaction Center-bound Cytochrome of *Rubrivivax gelatinosus**

Received for publication, February 18, 2004, and in revised form, May 12, 2004
Published, JBC Papers in Press, May 19, 2004, DOI 10.1074/jbc.M401784200

Jean Alric[¶]§¶, Makoto Yoshida^{||}, Kenji V. P. Nagashima^{||}, Rainer Hienerwadel[‡], Pierre Parot^{**},
André Verméglio[§], Shu-wen W. Chen^{‡‡}, and Jean-Luc Pellequer^{**§§}

From the [‡]Laboratoire de Génétique et Biophysique des Plantes, UMR 6191 CNRS-Commissariat à l'Énergie Atomique (CEA)-Aix-Marseille II, 163 avenue de Luminy, Marseille 13288, France, [§]CEA-Cadarache Direction des Sciences du Vivant (DSV)-Département d'Écophysiologie Végétale et de Microbiologie, Laboratoire de Bioénergétique Cellulaire, UMR 6191 CNRS-CEA-Aix-Marseille II, F-13108 Saint Paul lez Durance Cedex, France, the ^{||}Department of Biology, Tokyo Metropolitan University, Minamiohsawa 1-1, Hachioji, Tokyo 192-0397, Japan, ^{**}CEA-Valrhô, DSV-Département d'Ingénierie et d'Études des Protéines, Service de Biochimie post-génomique et Toxicologie Nucléaire, BP 17171, Bagnols sur Cèze 30207, France, and ^{‡‡}13 avenue de la Mayre, Bagnols sur Cèze 30200, France

The photosynthetic cyclic electron transfer of the purple bacterium *Rubrivivax gelatinosus*, involving the cytochrome *bc*₁ complex and the reaction center, can be carried out via two pathways. A high potential iron-sulfur protein (HiPIP) acts as the *in vivo* periplasmic electron donor to the reaction center (RC)-bound cytochrome when cells are grown under anaerobic conditions in the light, while cytochrome *c*₈ is the soluble electron carrier for cells grown under aerobic conditions in the dark. A spontaneous reversion of *R. gelatinosus* C244, a defective mutant in synthesis of the RC-bound cytochrome by insertion of a Km^r cassette leading to gene disruption with a slow growth rate, restores the normal photosynthetic growth. This revertant, designated C244-P1, lost the Km^r cassette but synthesized a RC-bound cytochrome with an external 77-amino acid insertion derived from the cassette. We characterized the RC-bound cytochrome of this mutant by EPR, time-resolved optical spectroscopy, and structural analysis. We also investigated the *in vivo* electron transfer rates between the two soluble electron donors and this RC-bound cytochrome. Our results demonstrated that the C244-P1 RC-bound cytochrome is still able to receive electrons from HiPIP, but it is no longer reducible by cytochrome *c*₈. Combining these experimental and theoretical protein-protein docking results, we conclude that cytochrome *c*₈ and HiPIP bind the RC-bound cytochrome at two distinct but partially overlapping sites.

In purple non-sulfur bacteria, electron transfer reactions involved in the conversion of light energy into biochemically amenable energy are performed by the photosynthetic apparatus. This complex system includes the photosynthetic reaction center (RC),¹ the cytochrome *bc*₁ complex, and water-soluble

electron carrier proteins in the periplasmic space and quinone molecules in the membrane. The primary process of photosynthetic electron transfer involves the RC in promoting the light-induced charge separation and stabilization, which results in oxidation of the primary electron donor P, the bacteriochlorophyll special pair, and reduction of a quinone to a semiquinone. Soluble electron carrier proteins transport electrons to the RC where the photo-oxidized special pair is rereduced. These soluble electron carriers are rereduced in turn by a quinol molecule via the cytochrome *bc*₁ complex. This so-called cyclic electron transfer occurring between these different electron carriers is coupled to proton translocation across the cytoplasmic membrane, creating a protonmotive force that drives ATP synthesis.

The RC is a transmembrane protein complex consisting of at least three polypeptides, namely the L, M, and H subunits. Apart from the three subunits, a fourth polypeptide, the C (cytochrome) subunit, is found on the periplasmic side of the RC in most purple bacteria. The fourth subunit, also known as the RC-bound cytochrome or tetraheme cytochrome, is a *c*-type cytochrome that accepts electrons from soluble electron carriers. In general, this RC-bound cytochrome contains four hemes differentiated by their redox properties: two hemes are high potential (HP), and two others are low potential (LP) (1, 2). However, one can also find merely three hemes in the RC-bound cytochrome in species such as *Rhodovulum sulfidophilum* (3–5). Three-dimensional structures of RC-bound cytochrome have been determined at high resolution for two purple bacteria, *i.e.* *Blastochloris* (formerly *Rhodopseudomonas*) *viridis* (6) and *Thermochromatium tepidum* (7). The four hemes are arranged linearly and labeled as starting from P, heme 1(III), heme 2(IV), heme 3(II), and heme 4(I). The spatial arrangement of the four hemes presents a high-low-high-low sequence in terms of redox potential² (1, 8, 9).

Two types of soluble electron carrier proteins have been shown to act as the electron donors to the RC-bound cytochrome. One is a *c*-type cytochrome. Several crystal structures of *c*-type cytochromes have been determined (10), including cytochrome *c* complexed with the cytochrome *bc*₁ (Protein Data Bank code 1KY0 (11)). The other type of soluble electron car-

* This work was supported by Commissariat à l'Énergie Atomique and in part by grants from the Ministry of Education, Science and Culture of Japan. The costs of publication of this article were defrayed in part by the payment of page charges. This article must therefore be hereby marked "advertisement" in accordance with 18 U.S.C. Section 1734 solely to indicate this fact.

¶ Supported by a research grant from Continuum Lasers.

§§ To whom correspondence should be addressed: CEA Valrhô-Centre de Marcoule, DSV/DIEP/SBTN-BP 17171, 30207 Bagnols sur Cèze, France. Tel.: 33-466-79-19-43; Fax: 33-466-79-19-05; E-mail: jlpellequer@cea.fr.

¹ The abbreviations used are: RC, reaction center; HiPIP, high potential iron-sulfur protein; HP, high potential; LP, low potential; WT, wild

type; MOPS, 4-morpholinepropanesulfonic acid; indel, inserted and deleted region; r.m.s.d., root mean square deviation.

² According to Ref. 44, roman numerals are used to denote the position of the heme binding motifs in the amino acid sequence starting from the N terminus, and arabic numerals indicate the structural position relative to the primary electron donor of the RC (see Fig. 8).

rier is an iron-sulfur protein (12, 13) that contains a [4Fe-4S] cluster. Due to the high redox midpoint potential compared with ferredoxins, this electron carrier was designated as "high potential" iron-sulfur protein or HiPIP. Several crystal structures for HiPIPs have been determined (10, 14). In species like *B. viridis* and *Rhodoblastus acidophilus*, only *c*-type cytochromes are found, e.g. either cytochrome c_2 or cytochrome c_8 . *Rubrivivax gelatinosus*, *Ectothiorhodospira shaposhnikovii*, *Rhodospirillum rubrum*, *Rhodococcus tenuis*, *Allochromatium vinosum*, and *Marichromatium purpuratum* utilize both types of electron transfer mediators, i.e. the HiPIP and the high potential *c*-type cytochrome. In *R. gelatinosus*, the HiPIP is the major electron donor to the RC under phototrophic anoxygenic growth conditions (15, 16), while the HP cytochrome c_8 becomes dominant when cells have been grown under dark aerobic conditions (17). Such adaptability in bioenergetic processes has also been found in *A. vinosum* (18).

Studies on *in vitro* electron transfer to the bound cytochromes modified by site-directed mutagenesis in *R. gelatinosus* have suggested that different amino acids of the RC-bound cytochrome are implicated in specific binding for the *c*-type cytochrome or HiPIP (19–21). These binding sites are located on the subunit surface close to the most distant accessible heme, the LP heme 4(I) (see also Ref. 22). A mutant strain, C244, lacking the RC-bound cytochrome was derived from the *R. gelatinosus* IL144 strain by inserting a kanamycin resistance cassette to inactivate the *pufC* gene (23). Although this mutant is able to grow under phototrophic condition, its growth rate is 4–5-fold decreased compared with the wild type. A spontaneous revertant strain, C244-P1, which presents a normal growth rate, was obtained from C244. The amino acid sequence of the C244-P1 RC-bound cytochrome shows that an insertion of 77 residues, originally from the kanamycin cassette, is located between residues 164 and 165 (in WT amino acid sequence) (24).

In the present work, we performed spectral, structural, and functional analysis on the RC-bound cytochromes from the WT and C244-P1 strains. The spatial arrangement of the four hemes in the RC-bound cytochrome was determined by EPR. The electron transfer mechanisms of the WT and C244-P1 strains were obtained by time-resolved optical spectroscopy. Our results showed that the spatial arrangement of the four hemes of the RC-bound cytochrome is not affected by the insertion of the 77 amino acids. On the other hand, this additional 77-residue segment in C244-P1 interferes with the binding of cytochrome c_8 but not HiPIP to the RC-bound cytochrome likely by spatially hindering the approach of cytochrome c_8 to its binding site. This led us to propose a comprehensive docking structure for identifying the binding sites for soluble electron carriers as well as the critical residues involved in binding and to construct the three-dimensional structure of the RC-bound cytochrome for the WT strain by comparative modeling.

EXPERIMENTAL PROCEDURES

C244-P1 Isolation and Growth—Cells of *R. gelatinosus* C244 strain, which was derived from the wild type strain IL144 and in which the gene coding the RC-bound cytochrome is disrupted by an insertion of a kanamycin resistance cassette (23), were photosynthetically grown in a PA medium containing 0.5% (w/v) sodium pyruvate, 20 mM potassium phosphate (pH 6.8), 1% (v/v) basal salt solution, 0.1% (v/v) vitamin solution (25), and 0.1% (w/v) ammonium sulfate. The photosynthetic growth rate of C244 cells was 4–5 times slower than that of the wild type cells. Continuous transfer of the growing cultures of C244 to the new medium containing no antibiotics resulted in appearance of revertant cultures showing nearly the same growth rates as that of the wild type culture. The revertant cells were isolated on solid medium containing 1.5% agar. One clone of the revertant cultures was named strain C244-P1.

Sample Preparations—Cells of *R. gelatinosus* WT IL144 and C244-P1

strains were grown under either dark aerobic or phototrophic anaerobic conditions in Hutner medium for 24 h. The altered *pufC* gene in the C244-P1 strain was sequenced and confirmed, through PCR amplification, by DNA sequence analysis using a 310 Genetic Analyzer (Applied Biosystems) (26). To obtain the membrane fraction, cells were harvested by centrifugation at $4000 \times g$ for 10 min, resuspended in 20 mM Tris-HCl at pH 8, and disrupted by French press at 50 megapascals. The remaining intact cells were separated from the membrane supernatant by centrifugation at $10,000 \times g$ for 10 min. The membrane fraction was then sedimented by ultracentrifugation at $250,000 \times g$ for 90 min and resuspended in 20 mM Tris-HCl at pH 7. HP cytochrome c_8 was purified as described previously (17) except for the use of a *R. gelatinosus* strain depleted for both HiPIP and the LP cytochrome c_8 . Cytochrome c_8 purity was checked by gel chromatography and monitoring the ratio between the absorption in the Soret band and at 280 nm.

EPR Spectroscopy—EPR spectra were taken at 15 K using a Bruker ER 300 X-band spectrometer equipped with an Oxford Instruments helium cryostat and a temperature control system. Instrumental conditions were set at 6.7-milliwatt microwave power, the microwave frequency was 9.43 GHz, and the modulation amplitude was 2.5 milliteslas. For EPR spectroscopy, membranes were diluted in a mixture of 20 mM MOPS and 2 mM ferricyanide at pH 7 to oxidize the heme groups, and the solution was pelleted and resuspended in 20 mM EDTA at pH 7 to remove manganese and ferricyanide. Finally the resulting membrane mixture was washed once more by centrifugation and resuspension in 20 mM MOPS at pH 7. Angular dependence of EPR signals was investigated on oriented membrane multilayer obtained by drying the membrane fragments onto Mylar sheets.

Time-resolved Spectroscopy—Time-resolved optical spectra were measured by a laboratory-built pulsed laser spectrophotometer with high sensitivity (27). The tunable laser source is a Surelite optical parametric oscillator (Continuum). The sample was photoexcited by a laboratory-made broadband dye laser pumped by a neodymium-yttrium aluminum garnet laser (LDS 821) with a wavelength range from 780 to 850 nm. The absorbance change in the cytochrome α -band was recorded in the time scale of ~ 100 ns to \sim s.

Construction of Molecular Three-dimensional Structures—We applied a comparative modeling strategy to build the framework of molecules. Alteration of backbone atomic positions was permitted only within inserted and deleted regions (indels). Side chains were replaced according to the corresponding protein sequence, and their atomic coordinates were minimized using our in-house program (28). Indels were built with computational graphics using the programs Turbo-Frodo (29) and Xfit (30). By this way, gaps of the backbone trace created by indels were filled by adjusting neighboring ϕ, ψ dihedral angles until the optimal bond length of the gap was reached. The atomic coordinates of final models were energy-minimized using X-PLOR 3.8 (31) with the Charmm22 all-atom force field parameters (32). Each comparative model was built in the presence of its native ligand, i.e. a *c*-type heme group for cytochrome c_8 and a [4Fe-4S] cluster for HiPIP. Appropriate patches were included when running X-PLOR to take into account thioester linkages in the *c*-type hemes. In this work, we built three comparative models from the species *R. gelatinosus*: the RC-bound cytochrome, cytochrome c_8 , and HiPIP.

We selected the RC-bound cytochrome of *T. tepidum* (Protein Data Bank code 1EYS (7)) as the template for our RC-bound cytochrome based on the global sequence alignment. It has fewer indels (four regions) and higher sequence identity (53%) to our molecular construction than *B. viridis* (Protein Data Bank code 1PRC (33)), which introduces eight indels and has lower sequence identity (49%). We used our superposition program, Sup3D, to perform superposition of 3D structures (28).

We used cytochrome c_{551} from *Pseudomonas aeruginosa* as the template for cytochrome c_8 . The two proteins share about 49% sequence identity. We selected the reduced form of c_{551} (Protein Data Bank code 451C (34)) to build the structural framework because it possesses the highest resolution (1.6 Å) and best R-factor (0.187) among all the c_{551} crystal structures in Protein Data Bank. According to multiple sequence alignments, residue Gly³⁹ in the template (451C) was deleted, and three residues were inserted at position 63 for cytochrome c_8 . Since the insertion region is near the heme and a conserved helix, we tilted the C-terminal helix to shift its N terminus away from the heme by about 2.6 Å such that there is enough space to accommodate the three inserted residues. We chose the crystal structure of HiPIP from *R. fermentans* (A chain in the Protein Data Bank code 1HLQ (35)) to build the model of the *R. gelatinosus* HiPIP. They share 60% sequence identity. The multiple sequence alignment indicates that only one residue inserted at position 47 is needed to accomplish the modeling.

Molecular Docking Simulations—Several interesting functional and structural features are shared by the cytochrome bc_1 complex and the RC-bound cytochrome complexed with soluble electron carriers. First, both bind with the same soluble cytochrome in the photosynthetic pathway. Second, both have a heme group partially exposed to solvent. Therefore, we assumed that the complex structure of the RC-bound cytochrome associated with cytochrome c_8 is similar in space to that of the yeast cytochrome bc_1 complex with its soluble cytochrome partner (Protein Data Bank code 1KYO (11)). Consequently docking of cytochrome c_8 to the RC-bound cytochrome was simulated based on the following. First, we superimposed atoms named FE, ND, NB, NC, and NA of the bc_1 heme group one-to-one onto FE, NA, NC, NB, and ND of heme 4(I) (see Fig. 7A below). This superposition placed the bc_1 cytochrome in a configuration similar to the RC-associated cytochrome, *i.e.* the His and Met axial ligands coincide in the two structures. Note that the sequence ordering of amino acids coordinated with the heme groups of the cytochrome bc_1 complex and the RC-bound cytochrome are reverse. Second, we superimposed cytochrome c_8 onto cytochrome c of 1KYO by mapping atoms FE, NA, NB, NC, and ND in the heme groups of both soluble cytochromes. The procedure put cytochrome c_8 at a plausible docking site on the surface of the RC-associated cytochrome. Third, armed with mutagenesis data (19), we developed a set of restrained distances between the side chain atoms of cytochrome c_8 and the RC-bound cytochrome. More explicitly, the distance restraint for atom CBC of heme 4(I) and that of the cytochrome c_8 heme is 5 Å. Similarly distances for atomic pairs Glu⁷⁹-O^{ε1}, Lys²¹-N^ε, and Glu⁹³-O^{ε1}, Lys⁸-N^ε are 3 and 5 Å, respectively.³ A rigid body energy minimization was performed by using the X-PLOR nuclear Overhauser effect statement to incorporate the distance restraints. We assigned the averaged interatomic distance to the center of a square-well potential function used in minimization. The ceiling of the potential was set to 1000 with a scaling factor of 10. Other running variables were by default.

Docking HiPIP was performed with computational graphics using InsightII (MSI Inc., San Diego, CA). We identified a large hydrophobic patch on the HiPIP surface formed by residues Leu¹⁵, Leu⁴³, Pro⁵⁶, Leu⁵⁷, Ala⁷¹, and Ala⁷³. We tested multiple orientations between the hydrophobic patch and two critical residues, Val⁶⁵ and Leu⁹⁴, of the RC-bound cytochrome (20, 21). We also carried out a rigid body energy minimization to refine the complex structure with various sets of distance restraints until the total potential energy was converged and shape complementarity was visually satisfactory. An additional set of distance restraints required for HiPIP docking includes 10 Å for Fe-3 of HiPIP and iron of the RC-bound cytochrome heme 4(I) group, 4 and 5 Å for atomic pairs Gln⁵⁵-C^δ, Leu⁴³-C^γ and Ser⁴⁶-C^β, Leu¹⁵-C^γ in the paired complex, respectively. We used the program BURIED, a variant of the MSMS software (36), for calculating the solvent-excluded surface. The value of the parameter density was set to 15. The atomic radii were taken from the CHARMM22 all-atom force field parameters. To obtain the non-polar and polar contributions, we separated the surfaces of carbon and sulfur atoms from that of oxygen and nitrogen atoms.

RESULTS AND DISCUSSION

Growth Rate and Genetic Analysis of C244-P1—The photosynthetic growth rate of *R. gelatinosus* strain C244 in which the gene coding for the RC-bound cytochrome, *pufC* gene, is disrupted by an insertion of a kanamycin resistance cassette was 4–5 times slower than that of the wild type in the growth medium used in this study. A revertant strain named C244-P1, obtained from the C244 cultures grown in the medium without kanamycin, restored the photosynthetic growth near to the level of that in the WT strain (Fig. 1A). Sequencing the *pufC* gene locus in C244-P1 showed that the kanamycin resistance cassette was lost except for 110 bases from the 5'-end and 121 bases from the 3'-end (Fig. 1, B and C). This means that 231 bases derived from the non-coding region of the cassette are included in the C244-P1 *pufC* gene. This insertion sequence does not contain any stop codons in the reading frame, meaning that the RC-bound cytochrome of C244-P1 has an external

77-amino acid insertion at the region between the HP heme 3(II) and LP heme 1(III) (Fig. 1C). We ascribed the reversion of the photosynthetic growth in C244-P1 to the recovery of synthesis of the RC-bound cytochrome, although the sequence was altered from WT.

Functional and Structural Analysis of WT and C244-P1 RC-bound Cytochromes—To investigate how the RC-bound cytochrome transfers an electron to the primary electron donor, spectroscopic measurements on IL144 and C244-P1 whole cells grown under phototrophic anaerobic conditions were performed. Anaerobic dark adaptation of the sample allows the reduction of all four hemes prior to excitation. Under these conditions, excitation by a saturating flash induces the photo-oxidation of the LP hemes. A continuous illumination of low intensity photo-oxidizes the two LP hemes but leaves the two HP hemes reduced. A superimposed excitation by a saturating flash under these conditions induces the photo-oxidation of the HP hemes. The time-resolved flash-induced absorbance changes for the dark-adapted IL144 and C244-P1 samples are presented in Fig. 2, A and B, respectively. For an anaerobic dark-adapted sample, the decrease in absorbance peaking at 552 nm is indicative of photo-oxidation of the LP hemes of RC-bound cytochrome concomitant with the reduction of the photo-oxidized primary donor. When the sample was exposed to far red light ($\lambda > 700$ nm) of 50 milliwatts·cm⁻² (Fig. 2, D and E), photo-oxidation of a cytochrome peaking at 555 nm was observed. This is indicative of the photo-oxidation of the HP hemes. Fig. 2, C and F, shows that the interheme electron transfer involving either the LP or the HP hemes is identical for the WT and the C244-P1 strains.

The spatial arrangement of the hemes in the WT and C244-P1 RC-bound cytochromes was determined by EPR spectroscopy. For the fully oxidized C244-P1 RC-bound cytochrome, the angular dependent EPR signal with the g_z -value of 3.15 has the maximal amplitude along the angle 0°, indicating that the plane of a HP heme is perpendicular to the membrane (Fig. 3, A and B). Two weak signals, at the g_z -value of 3.4, have their maximal amplitudes along angles 0° and 90° (Fig. 3, A and C). This finding is consistent with the expected g_z -values between 3.3 and 3.4 for three other hemes. The EPR results for C244-P1 are similar to that for the WT IL144 (data not shown and Ref. 2). They indicate that the heme groups from the two strains are spatially arranged in a similar manner.

Functional Characterization of RC-bound Cytochrome-HiPIP Interaction in Different Strains—For the IL144 cells grown under photosynthetic conditions, the HP hemes are reduced with a half-time of about 300 μs by HiPIP (15–17). Fig. 4A presents comparisons of *in vivo* kinetics of the rereduction rate of the HP hemes for the WT IL144, the C244-P1 revertant, and ΔHiPIP, a mutant lacking HiPIP (16). No fast phase of the bound cytochrome rereduction is observed for the ΔHiPIP mutant as already published (16). The rate of rereduction of the HP hemes can be fitted with a fast phase of 290 μs with a relative amplitude of 0.39 in the case of WT, consistent with the results reported previously (15). In the case of the C244-P1 mutant, we obtained a longer half-time of 530 μs with an amplitude of 0.33. The similar amplitude for both fast phases indicates that HiPIP rereduces the HP hemes of RC-bound cytochromes of IL144 and C244-P1 to a similar extent. On the other hand, the electron transfer rate for C244-P1 is ~2-fold slower than that for IL144. The *in vitro* experiments (Fig. 4B) confirm that HiPIP readily interacts with the C244-P1 RC-bound cytochrome: the rereduction of the RC-bound cytochrome is achieved when HiPIP concentrations in the C244-P1 membrane suspension are increased. The observed electron transfer rate k_{obs} is found to vary hyperbolically with the con-

³ There is a discrepancy in the literature about the residue numbering in *R. gelatinosus*. In Refs. 19–21, experiments were performed on *R. gelatinosus*, while the numbering was borrowed from *B. viridis*. Thus, published mutants Val⁶⁷, Glu⁷⁹, Glu⁹³, and Leu⁹⁶ correspond to *R. gelatinosus* residues Val⁶⁵, Glu⁷⁷, Glu⁹¹, and Leu⁹⁴, respectively.

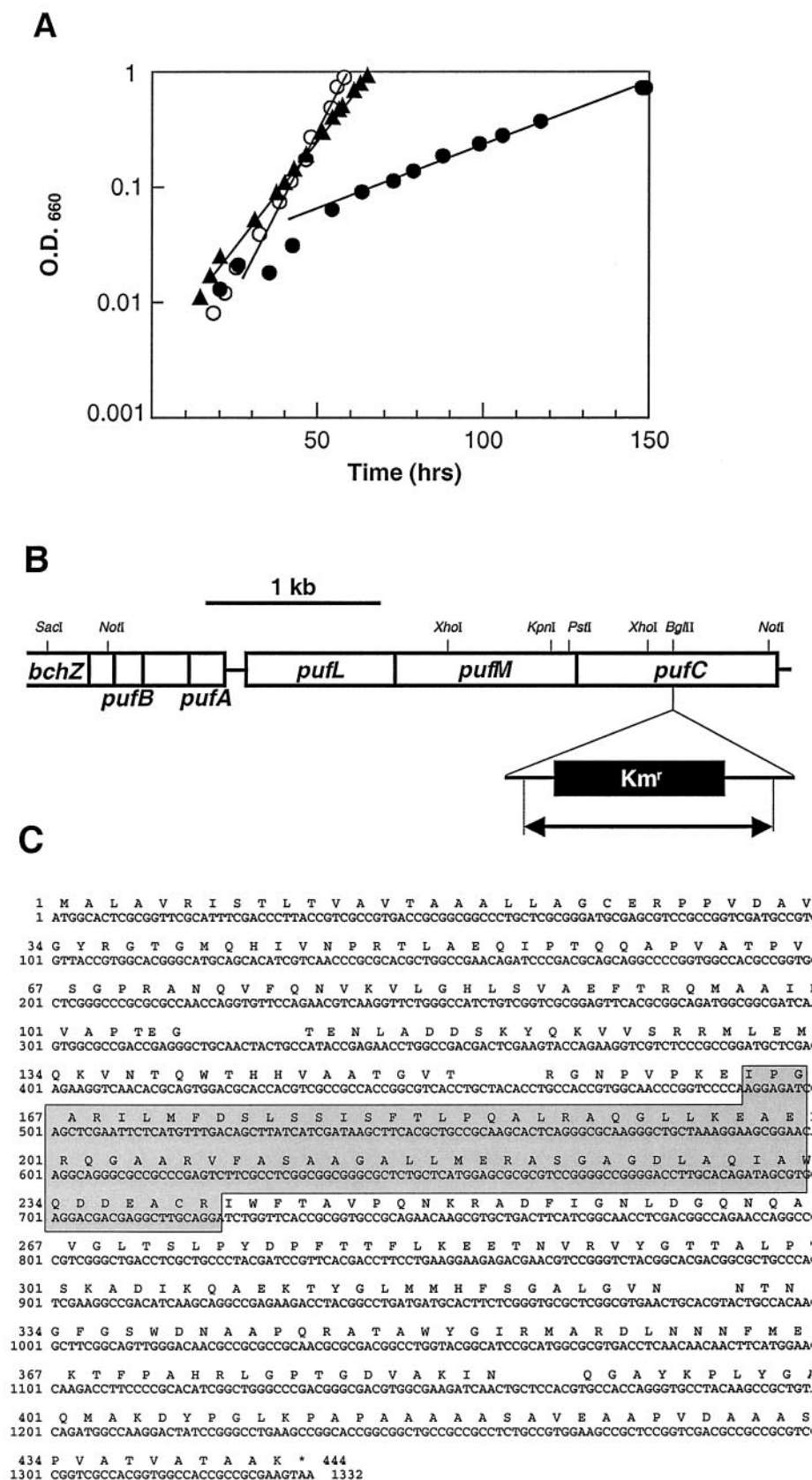


FIG. 1. Characteristics of *R. gelatinosus* strain C244-P1. **A**, photosynthetic growth of *R. gelatinosus* IL144, C244, and C244-P1. The growth of the bacteria was measured by optical density at 660 nm. Doubling times were calculated to be 5.9 h for WT (○), 28.5 h for C244 (●), and 8.1 h for C244-P1 (▲). **B**, schematic representation of *puf* operon in C244, the parent strain of C244-P1. The *pufC* gene of C244 contains a kanamycin resistance cartridge at a unique BglII restriction site. A horizontal arrow below the cartridge shows the region lost in the *pufC* locus in C244-P1. **C**, nucleotide sequence of *pufC* gene in C244-P1. The 231-base insertion derived from the non-coding region of the kanamycin resistance cartridge is shaded. The deduced amino acid sequence is also presented above the nucleotide sequence. Four binding motifs for hemes are shown in reverse contrast.

FIG. 2. Difference absorption spectra in the α -band of cytochromes. Spectra recorded at various times after light excitation for the WT IL144 (A and D) or C244-P1 (B and E) whole cells placed either under dark-adapted anaerobic conditions (A and B, LP hemes reduced before the flash) or in the presence of a continuous near infrared light of 50 milliwatts \cdot cm $^{-2}$ (D and E, only HP hemes reduced before the flash). The kinetics of cytochrome oxidation under HP or LP (C and F) are plotted for better comparison. *r.u.*, renormalized units.

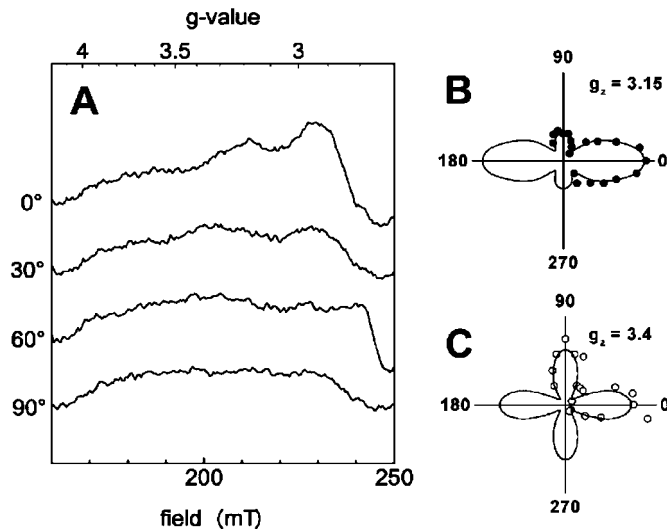
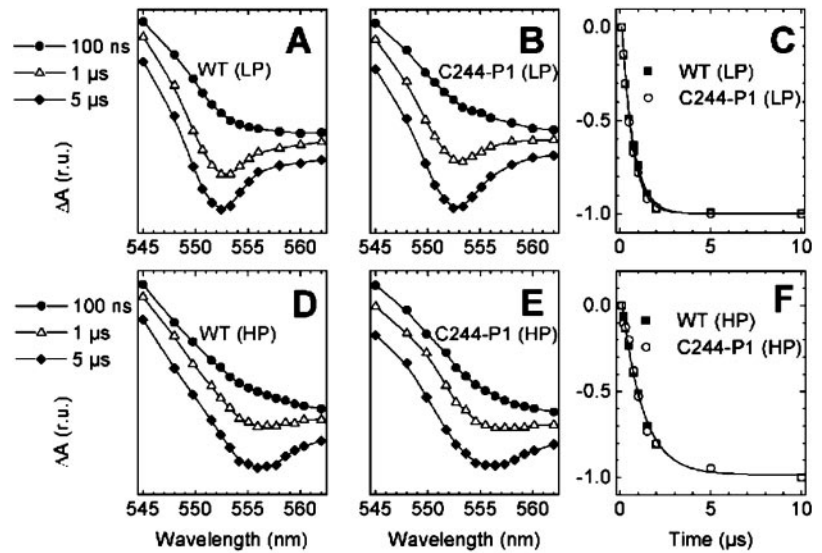


FIG. 3. Orientation dependence of EPR spectra recorded at 15 K on *R. gelatinosus* C244-P1 oriented membrane fragments previously oxidized by ferricyanide addition. Angles are given between the plane of the multilayer and the direction of the magnetic field. A g_z peak at 3.15 for the +300 mV heme as well as signals at 3.3 and 3.4 for the other hemes have been identified previously (2). *mT*, milliteslas.

centration of HiPIP (Fig. 4C), and the data are fitted to the equation below (37),

$$k_{\text{obs}} = k_{\text{et}}[\text{HiPIP}]/(K_d + [\text{HiPIP}]) \quad (\text{Eq. 1})$$

where $K_d = 13 \mu\text{M}$ is the dissociation constant and $k_{\text{et}} = 40 \text{ s}^{-1}$ is the specific electron transfer rate constant. When compared with the values obtained for WT ($K_d = 5.7 \mu\text{M}$ and $k_{\text{et}} = 74.4 \text{ s}^{-1}$ (15)), these data confirm the small alteration of electron transfer rate already observed on whole cells (Fig. 4A) and the slightly lower affinity of HiPIP for the C244-P1 RC-bound cytochrome than for WT.

Functional Characterization of RC-bound Cytochrome-Cytochrome c_8 Interaction in the WT and the C244-P1 Mutant—Menin and co-workers (17) have found that IL144 cells grown aerobically produce a large amount of cytochrome c_8 , which acts as an efficient electron donor to the HP hemes of the RC-bound cytochrome. The interaction between the RC-bound cytochrome and cytochrome c_8 was therefore studied on cells grown under these dark aerobic conditions. The presence of HP cytochrome c_8 in the periplasm of C244-P1 was first confirmed

by monitoring the amount of cytochromes in the soluble fraction. The relative amount of HP and LP cytochrome c_8 was determined by comparing absorption spectra for ascorbate-reduced (HP cytochrome reduced) or dithionite-reduced (both HP and LP cytochromes reduced) samples. The ratio between the extents of redox absorbance changes at 550 nm was found to be equal to 3:1 for C244-P1 as already reported for the WT IL144 (17). Fig. 5, A and B, presents the light-induced absorbance changes in the cytochrome α -band for IL144 and C244-P1 intact cells. The spectra taken at 50 μs and 7 ms after the actinic flash are shown together with their difference. The HP hemes of both strains are photo-oxidized as indicated by the downward peaks at 556 nm in the 50- μs spectrum. In the case of WT, the peak is shifted to shorter wavelengths after 7 ms, indicative of rereduction of the RC-bound cytochrome by cytochrome c_8 (17). This intercytochrome electron transfer process is characterized by an upward peak at 550 nm and a downward peak at 557 nm observed in the spectral difference between the two elapsed times. The absorbance changes between 550 and 557 nm are indicative of the rate of electron transfer between cytochrome c_8 and the RC-bound cytochrome (Fig. 6A). In the case of WT (Fig. 6A, closed squares), the fitted half-time is 390 μs in agreement with a previous report (17). On the other hand, no spectral shift was observed for the C244-P1 mutant between 50 μs and 7 ms (Fig. 5B), and no fast electron transfer was observed between the cytochrome c_8 and the RC-bound cytochrome (Fig. 6A, open circles). In reconstitution experiments with endogenous cytochrome c_8 , we observed that the electron transfer between this cytochrome and the RC-bound tetraheme cytochrome was significantly inefficient in C244-P1 compared with WT (Fig. 6B). We therefore conclude that electron transfer from cytochrome c_8 to the RC-bound cytochrome is strongly inhibited in the C244-P1 mutant. However, when cells were shifted from dark aerobic to photoautotrophic anaerobic conditions, no significant difference could be observed in the growth curve of C244-P1 compared with WT. The two strains showed similar lag time (2–4 h) and doubling time (6 and 8 h) suggesting that an efficient photosynthetic activity does not increase significantly the adaptation capability of the cells.

Structural Analysis of the RC-bound Cytochrome of WT and C244-P1—The unchanged redox potentials of the hemes in both IL144 and C244-P1 (data not shown) and their similar arrangement as well as the identical time dependence of inter-heme electron transfer discussed above infer that the function of RC-bound cytochromes is conserved in the two strains. From structural analysis on the RC-bound cytochromes of *B. viridis*

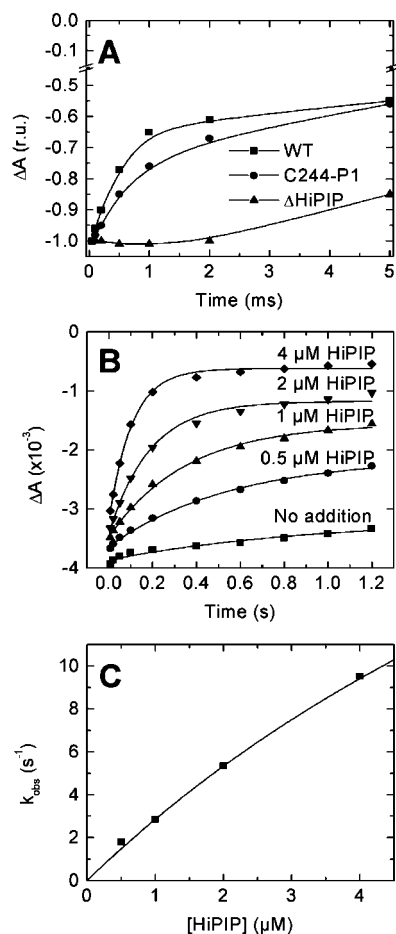


FIG. 4. **A**, time-resolved flash-induced absorbance changes recorded at 422 nm on a suspension of C244-P1 (●) or IL144 (■) whole cells placed under aerobic conditions. For the mutant lacking HiPIP (16), the kinetics of the re-reduction of the RC-bound cytochrome are plotted for comparison (▲). **B**, reconstitution experiments of ascorbate-reduced C244-P1 membrane fragments supplemented with HiPIP. **C**, plot of the observed electron transfer rate k_{obs} between HiPIP and the RC-bound cytochrome in function of the concentration of HiPIP (values taken from the reconstitution experiment of **B**). The data were fitted to equation $k_{\text{obs}} = k_{\text{et}} [\text{HiPIP}] / (K_d + [\text{HiPIP}])$ with an electron transfer rate of $k_{\text{et}} = 40 \text{ s}^{-1}$ and a dissociation constant of $K_d = 13 \text{ } \mu\text{M}$. *r.u.*, renormalized unit.

(6, 33) and *T. tepidum* (7), we show below that, despite the 77-amino acid insertion, the retrieval of a functional RC-bound cytochrome in C244-P1 is compatible with a reliable folding of the protein.

The three dimensional structures of the RC-bound cytochromes from *B. viridis* (1PRC) (6, 33) and *T. tepidum* (1EYS) (7) have revealed that their N-terminal and C-terminal domains form a pseudo twofold symmetry. Each domain bears two heme groups and is referred to as a diheme. The overall fold of the structure of the RC-bound cytochrome from these species is well conserved except for that in a long loop region joining the two dihemis provoking high flexibility in the local conformation. The loop in *B. viridis* (1PRC), residues 148–189, is longer than the loop in *T. tepidum* (1EYS), residues 147–177; and while both loops are located near the membrane, they point in different directions (Fig. 7B). Knowing that the additional 77-residue insertion in the C244-P1 RC-bound cytochrome occurs within this loop region (Fig. 1C), we anticipated that this insertion does not impair the core structure of the subunit. We therefore conclude that the only structural difference between WT and the C244-P1 mutant is a protruding loop extending over the RC-bound cytochrome. Thus we can borrow the three-

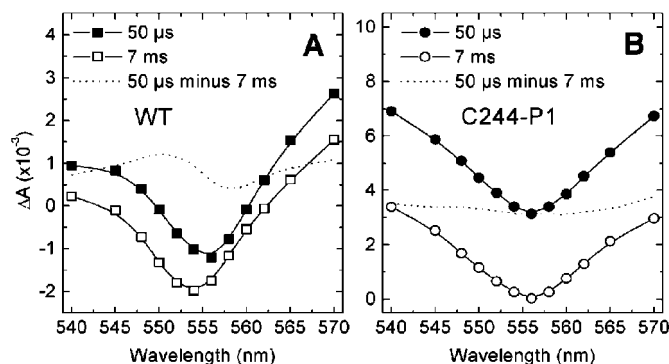


FIG. 5. **Time-resolved spectra of photoinduced absorption changes in the α -band of cytochromes obtained on dark aerobically grown whole cells of *R. gelatinosus* IL144 (A) and C244-P1 (B) placed under aerobic conditions (HP). The spectra at 50 μs (●) and 7 ms (○) and the difference between them (dashed line) are displayed.**

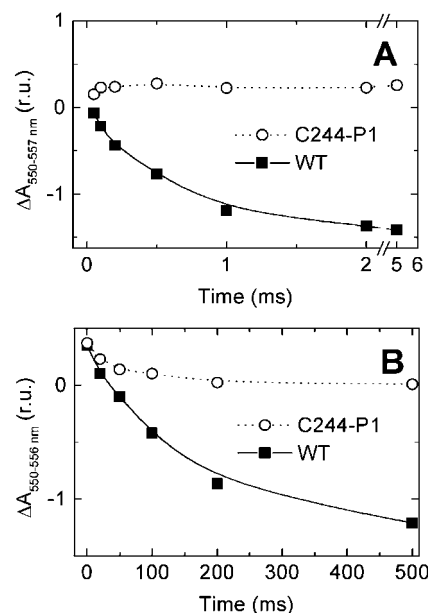
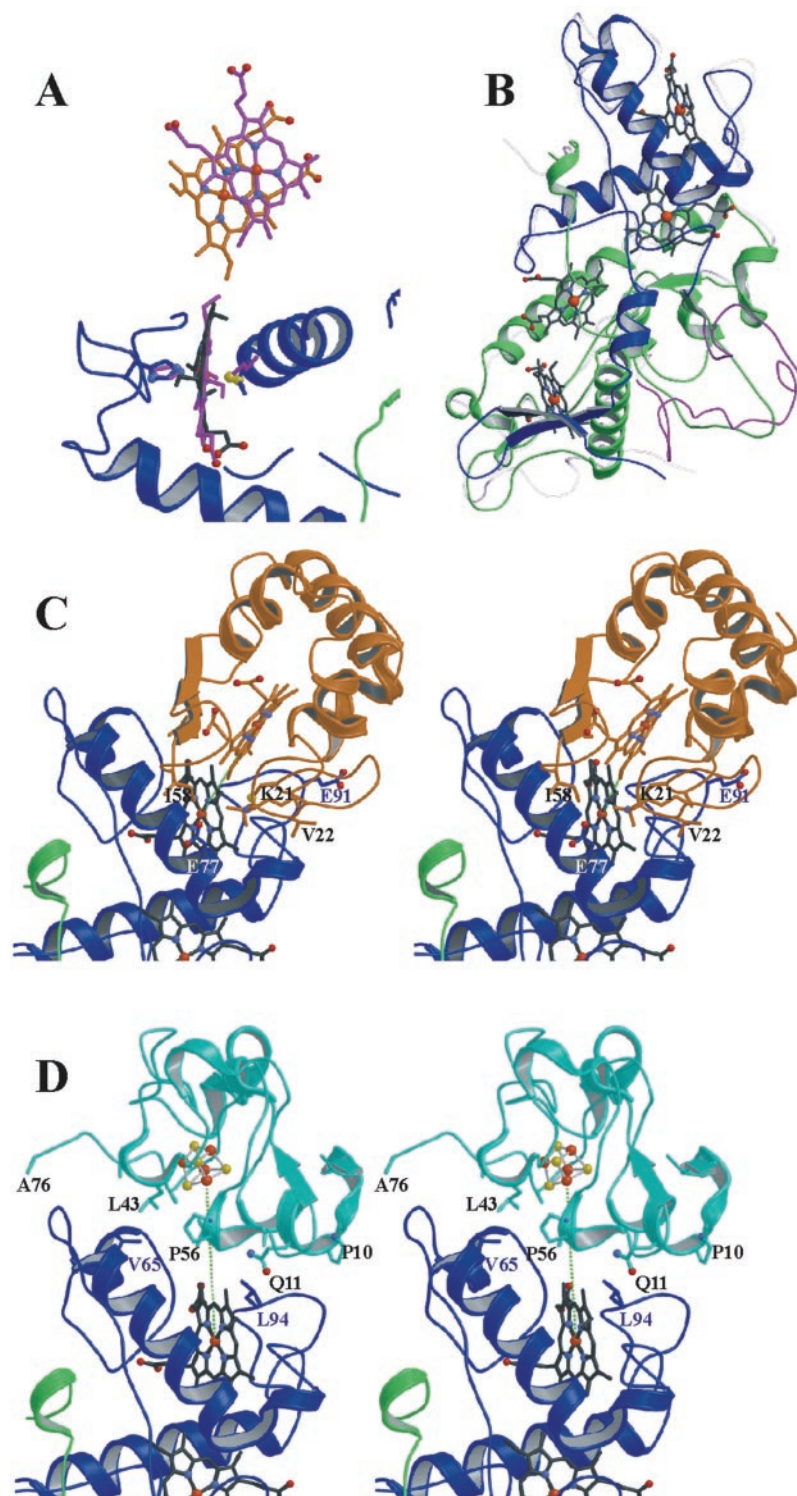


FIG. 6. **In vivo** kinetics of light-induced electron transfer between the soluble cytochrome c_3 and the RC-bound cytochrome in dark aerobically grown cells of *R. gelatinosus* IL144 and C244-P1 (A). **In vitro** kinetics of light-induced electron transfer between the soluble cytochrome c_3 and the RC-bound cytochrome in reconstitution experiments are shown. The concentration in RC was adjusted to 1 μM . Ascorbate-reduced membrane fragments of *R. gelatinosus* IL144 or C244-P1 were supplemented with 1 μM endogenous cytochrome c_3 (B). The light-induced absorbance changes were monitored in the α -band of cytochromes for both *in vivo* and *in vitro* experiments. *r.u.*, renormalized unit.

dimensional structure from WT for C244-P1 to investigate the interaction between the RC-bound cytochrome and soluble electron carriers. The quality of the *R. gelatinosus* RC-bound cytochrome model was examined by PROCHECK (38). The modeled structure possesses 77% of ϕ, ψ dihedral angles in the most favored region, while the template 1EYS has 79%. The decreased accuracy from the model is mainly due to three insertions in the loops near the membrane; nevertheless these insertions are distant from the docking patch. Another cause arises from increasing backbone strains in neighboring residues around the deletion at Gly⁹². Fortunately this unfavorable deviation is minute and would not significantly influence the docking outcome. The quality of our model can be further strengthened by the Sup3D results, which yielded a root mean square deviation (r.m.s.d.) value of 0.12 Å by superimposing 303 C_α atoms of the model with the template, providing the full

FIG. 7. Schematic representation of molecular models. A, superposition of the RC-bound cytochrome model from *R. gelatinosus* (blue and green) and the heme 1 group from the yeast *bc₁* complex (magenta). Axial ligands from hemes are drawn in balls and sticks where sulfur atoms are yellow. In this orientation, the bound soluble cytochrome from the *bc₁* complex is oriented as shown in magenta (top). The modeled heme of the cytochrome *c₈* from *R. gelatinosus* is shown in gold (top). B, superposition of the RC-bound cytochrome from *T. tepidum* (green and blue) and *B. viridis* (plain and transparent magenta). Secondary structure elements are shown as coils for helices and arrows for β -strands. The four heme groups of *T. tepidum* are drawn in balls and sticks in which carbons are omitted, nitrogen atoms are blue, oxygen atoms are red, and iron atoms are orange. Both RC-bound cytochrome molecules superposed well on their entire sequence except in a long loop connecting the two di-heme segments located on the bottom right. Pictures were generated by Molscript and rendered by Raster3D. C, stereo three-dimensional representation of a molecular docking between *R. gelatinosus* RC-bound cytochrome (blue and green) and *R. gelatinosus* cytochrome *c₈* (gold). Several residues involved in direct contacts are indicated. The distance between the two iron atoms is 15 Å and is represented by green dots. D, stereo three-dimensional representation of a molecular docking between *R. gelatinosus* RC-bound cytochrome (blue and green) and *R. gelatinosus* HiPIP (cyan). The [4Fe-4S] cluster is drawn as balls and sticks using yellow for sulfur and orange for iron. Several residues involved in direct contacts are indicated. The distance between the closest iron atom from the cluster and the iron from the heme iron is 14 Å and is represented by green dots. The figure was drawn with Molscript (45) and rendered with Raster3D (46).



protein length is 311 residues. Likewise superimposing 270 residues of the model with 1PRC (*B. viridis*) gave a r.m.s.d. of 0.96 Å.

Structural Analysis of Soluble Electron Donors—Comparative models for both soluble electron donors were built as described under “Experimental Procedures.” The quality of the HiPIP model was determined by PROCHECK to yield 89% of ϕ, ψ dihedral angles in the most favored region, the same as its template, 1HLQ:A. The Sup3D results yielded a C_{α} -r.m.s.d. value of 0.26 Å for HiPIP with 75 residues (*i.e.* the full length) superimposed. For soluble cytochromes, PROCHECK found 85% for the model of cytochrome *c₈* and 93% for the template,

cytochrome *c₅₅₁*. The lost accuracy in the cytochrome *c₈* model is primarily due to the three-residue insertion; otherwise it is closely matched with the template. Especially the hydrophobic patch surrounding the heme group in the cytochrome *c₈* model is structurally equivalent to the template. We obtained a C_{α} -r.m.s.d. value of 0.26 Å for cytochrome *c₈* by superimposing 69 of 82 residues and 2.3 Å with the full length. We found that the much greater C_{α} -r.m.s.d. value with the full length for cytochrome *c₈* is due to the shifting of the C-terminal helix. We also noticed that cytochrome *c₈* contains more Lys residues than the template, 12 *versus* 8. The excessive Lys residues provoke dramatic change in electrostatic

TABLE I
Buried molecular surface areas

| Pair of molecules | Buried surface area ^a | | Critical residue-residue interactions |
|--|----------------------------------|---------|---|
| | Non-polar | Polar | |
| RC-bound cytochrome/ cytochrome <i>c</i> ₈ | 285/390 | 157/72 | Thr ⁶⁹ /Ile ⁶¹ Glu ⁷⁷ /Lys ²¹ Glu ⁷⁷ /Val ²³ Glu ⁷⁷ /Ile ⁵⁸ Pro ⁸¹ /Val ²² Thr ⁸² /Val ²² Cys ⁸⁵ /Ala ¹⁴ Cys ⁸⁵ /Cys ¹⁵ Asn ⁸⁶ /Ala ¹⁴ Glu ⁹¹ /Lys ⁸ |
| RC-bound cytochrome/ HiPIP | 305/333 | 117/106 | Ser ⁴⁶ /Ala ⁷⁶ Pro ⁴⁸ /Ala ⁷³ Val ⁵³ /Ala ⁷¹ Phe ⁵⁴ /Leu ⁵⁷ Gln ⁵⁵ /Ala ¹⁴ Val ⁶⁵ /Leu ⁴³ Thr ⁶⁹ /Pro ⁵⁶ Glu ⁹¹ /Pro ¹⁰ Leu ⁹⁴ /Gln ¹¹ Heme 4(I)/Leu ⁵⁷ |
| 1KYO-O/1KYO-W ^b | 266/261 | 120/151 | |

^a The contribution to the buried surface area is decomposed for each partner in the unit of Å².

^b The last letter indicates the Protein Data Bank chain in the crystal structure; O corresponds to cytochrome *c*₁, and W corresponds to the bound cytochrome *c*.

properties with a net charge of +5e in cytochrome *c*₈ compared with −1e in the template.

Structural Analysis of Docking Models—Having three-dimensional structures for the RC-bound cytochrome as well as for both soluble electron donors, it was now possible to dock these molecules onto each other as described under “Experimental Procedures.” Experimental facts infer that interaction between the RC-bound cytochrome and HiPIP is through their solvent-exposed hydrophobic regions. For example, mutagenesis results have shown that Val⁶⁵ (21) and Leu⁹⁴ (20) of the RC-bound cytochrome are critical for binding with HiPIP. Mutating hydrophobic amino acids in this region exerts stronger effects than other types of amino acids on RC-bound cytochrome-HiPIP binding strength (21). From our predicted RC-bound cytochrome-HiPIP complex (Fig. 7C), the non-polar solvent-excluded surfaces on the docking patch are 305 Å² (72%) and 333 Å² (76%) for the RC-bound cytochrome and HiPIP, respectively. It implies that the binding of the RC-bound cytochrome with HiPIP is predominated by the non-polar interaction. Among them, the heme 4(I) of the RC-bound cytochrome interacts with Leu⁵⁷ of HiPIP. Characterization of the structure of the complex, RC-bound cytochrome-HiPIP, is described in Table I. A recent study on the *A. vinosum* species has identified a critical residue in HiPIP for electron transfer to the RC-bound cytochrome, Phe⁴⁸, corresponding to Leu⁴³ in *R. gelatinosus* (39). Their results corroborate our docking data in which Leu⁴³ occupies a central location in the HiPIP hydrophobic patch and is located at the interface with the *R. gelatinosus* RC-bound cytochrome.

The structural model of the RC-bound cytochrome complexed with cytochrome *c*₈ is shown in Fig. 7D. Two critical residues revealed from mutagenesis, Glu⁷⁷ and Glu⁹¹ of the RC-bound cytochrome (19), form very favorable salt bridges with Lys²¹ and Lys⁸/Lys⁹ of cytochrome *c*₈, respectively. Alteration in these two residues influences the magnitude of the second-order rate constant of the RC-bound cytochrome-cytochrome *c*₈ reaction (19). Although to a smaller extent, a third residue, Glu⁸³ of the RC-bound cytochrome, appears to be involved in binding with cytochrome *c*₈. Structural analysis revealed this residue to be surrounded by residues Gln¹⁷ and Lys²⁰ of cyto-

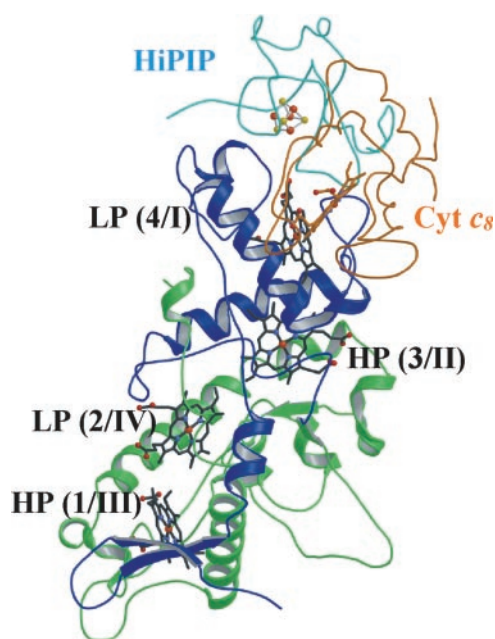


FIG. 8. Schematic drawing of the *R. gelatinosus* soluble electron donor (gold for cytochrome *c*₈ and cyan for HiPIP) docked onto the *R. gelatinosus* RC-bound cytochrome (green and blue) where heme groups are labeled (see Footnote 2). This view clearly shows the two exclusively overlapping binding sites: on the top left for HiPIP and on the top right for cytochrome (Cyt) *c*₈.

chrome *c*₈; however, they are not in the salt bridge interaction range. Note that the side chains of these residues were not further refined. Cys⁸⁵ of the RC-bound cytochrome was found to interact with the cytochrome *c*₈ heme. Characterization of the complex RC-bound cytochrome-cytochrome *c*₈ is also described in Table I. The non-polar solvent-excluded surfaces are 390 Å², which is 84% of the total amount. The magnitude is larger than that for complex *bc*₁-cytochrome *c*, which is 261 Å² corresponding to 69% of the total. It is also larger than two other complexes, the *Rhodobacter sphaeroides* RC (330 Å², 57%) (40) and the cytochrome *c* peroxidase (313 Å², 62%) (41) bound with soluble cytochromes. In addition, the buried surface ratios of non-polar to polar are almost identical for RC-bound cytochrome-cytochrome *c*₈ (1.82) and the yeast *bc*₁-cytochrome *c* (1.76) complexes. It suggests that the two molecular pairs have similar binding orientations. Moreover, it also shows that the interaction between the RC-bound cytochrome and cytochrome *c*₈ is more polar than the three other cases in comparison. Analysis of the docking models of RC-bound cytochrome-HiPIP and RC-bound cytochrome-cytochrome *c*₈ showed that iron atom of the cytochrome *c*₈ heme is about 14 Å away from the [4Fe-4S] cluster of HiPIP (see Fig. 7). When we superimposed the docking complexes of both soluble electron donor onto the RC-bound cytochrome, it was easily seen that they are partially overlapping binding sites (Fig. 8).

The electron transfer theory (42) describes the electron transfer rate as a function of a geometric parameter, the edge-to-edge distance between two redox cofactors. To apply this theory to RCs interacting with soluble redox proteins in photosynthesis, we related the estimated half-time (*t*_{1/2}) of electron transfer between two hemes and the interheme distance through the following empirical equation (43),

$$\log_{10}k_{\text{et}} = 13 - 0.6(R - 3.6) - 3.1(-\Delta G + \lambda)^2/\lambda - \Delta G/0.06 \quad (\text{Eq. 2})$$

where *k*_{et} (in s^{−1}) is the electron transfer rate (with *t*_{1/2} = ln2/*k*_{et}), Δ*G* (in eV) is the free energy of the reaction, λ (in eV) is the reorganization energy, and *R* (in Å) is the edge-to-edge

distance between cofactors. As suggested previously (19), our docking model reflects the rereducing process that is apparently energetically unfavorable but still possible according to the aforementioned theory. The predicted edge-to-edge distance between the iron/sulfur redox center of the HiPIP and the heme 4(I) of the RC-bound cytochrome is 8.84 Å (between sulfur S-4 and carbon CMA, respectively). The redox potential of *R. gelatinosus* HiPIP is + 330 mV, and the lowest potential heme of the RC-bound cytochrome titrates at + 70 mV. The free energy between the two cofactors is thus 0.26 eV. The rate of the uphill electron transfer between HiPIP and the RC-bound cytochrome could be determined using the above described empirical formula. A reorganization energy of 1.16 eV allows a half-time of 300 μs as it has been determined experimentally on WT. The λ value is slightly higher than the commonly used 1 eV for an interprotein electron transfer. This probably arises from more dramatic rearrangement of solvent molecules along the electron transfer pathway. Assuming that none of the parameters except the distance change in the C244-P1 mutant, we can ascribe a distance enlargement of 0.4 Å to the increase of the half-time from 300 to 500 μs. We conclude from the small increase of the distance between the two redox centers that the additional loop does not modify dramatically the binding of HiPIP onto the RC-bound cytochrome, consistent with the dissociation constant above determined.

Conclusions—In the present work, we have shown by EPR experiments, fast light-induced interheme electron transfer and molecular modeling that electron transfer from two soluble electron donors, HiPIP and cytochrome *c*₈, to the *R. gelatinosus* RC-bound cytochrome occurs via two interacting pathways.

Contrary to WT where both HiPIP and cytochrome *c*₈ are efficient electron donors to the RC-bound cytochrome, time-resolved spectroscopy and reconstitution experiments indicated that electron transfer to the C244-P1 RC-bound cytochrome occurs from HiPIP but not from cytochrome *c*₈. The protein-protein docking results of the *R. gelatinosus* WT RC-bound cytochrome complexed with either HiPIP or cytochrome *c*₈ revealed that the two soluble electron donors interact at two exclusively overlapping binding sites. Structural and sequence analysis on the present molecular models as well as crystal structures from *B. viridis* and *T. tepidum* RCs showed that the three-dimensional structure of the RC-bound cytochrome is alike in WT and the C244-P1 mutant except for the highly flexible loop between the two diheme domains containing an additional 77-residue insertion in the latter. It suggests that the lengthened loop in C244-P1 may adopt an *ad hoc* orientation to selectively block the interaction with cytochrome *c*₈ but not with HiPIP. This arrangement was a requisite since the revertant strain had recovered a fast growth rate under photosynthetic conditions where HiPIP is the preferential donor to the RC-bound cytochrome.

Acknowledgments—We thank W. Nitschke and B. Schoepp-Cothenet (CNRS, Marseille, France) for EPR measurements, helpful discussions, and critical reading of the manuscript.

REFERENCES

- Nitschke, W., and Rutherford, A. W. (1989) *Biochemistry* **28**, 3161–3168
- Nitschke, W., Agalidis, I., and Rutherford, A. W. (1992) *Biochim. Biophys. Acta* **1100**, 49–57
- Masuda, S., Yoshida, M., Nagashima, K. V., Shimada, K., and Matsuura, K. (1999) *J. Biol. Chem.* **274**, 10795–10801
- Yoshida, M., Masuda, S., Nagashima, K. V., Vermeglio, A., Shimada, K., and Matsuura, K. (2001) *Biochim. Biophys. Acta* **1506**, 23–30
- Masuda, S., Tsukatani, Y., Kimura, Y., Nagashima, K. V., Shimada, K., and Matsuura, K. (2002) *Biochemistry* **41**, 11211–11217
- Deisenhofer, J., Epp, O., Miki, K., Huber, R., and Michel, H. (1985) *Nature* **318**, 618–624
- Nogi, T., Fathir, I., Kobayashi, M., Nozawa, T., and Miki, K. (2000) *Proc. Natl. Acad. Sci. U. S. A.* **97**, 13561–13566
- Vermeglio, A., Richaud, P., and Breton, J. (1989) *FEBS Lett.* **243**, 259–263
- Alegria, G., and Dutton, P. L. (1991) *Biochim. Biophys. Acta* **1057**, 258–272
- Messerschmidt, A., Huber, R., Poulos, T., and Wieghardt, K. (eds) (2001) *Handbook of Metalloproteins*, Vol. 1, pp. 33–43, John Wiley & Sons, Chichester, UK
- Lange, C., and Hunte, C. (2002) *Proc. Natl. Acad. Sci. U. S. A.* **99**, 2800–2805
- Kerfeld, C., Chan, C., Hirasawa, M., Kleis-SanFrancisco, S., Yeates, T., and Knaff, D. (1996) *Biochemistry* **35**, 7812–7818
- Hochkoeppler, A., Zannoni, D., Ciurli, S., Meyer, T., Cusanovich, M., and Tollin, G. (1996) *Proc. Natl. Acad. Sci. U. S. A.* **93**, 6998–7002
- Nogi, T., and Miki, K. (2001) *J. Biochem.* **130**, 319–329
- Schoepp, B., Parot, P., Menin, L., Gaillard, J., Richaud, P., and Vermeglio, A. (1995) *Biochemistry* **34**, 11736–11742
- Nagashima, K. V., Matsuura, K., Shimada, K., and Vermeglio, A. (2002) *Biochemistry* **41**, 14028–14032
- Menin, L., Yoshida, M., Jaquinod, M., Nagashima, K. V., Matsuura, K., Parot, P., and Vermeglio, A. (1999) *Biochemistry* **38**, 15238–15244
- Vermeglio, A., Li, J., Schoepp-Cothenet, B., Pratt, N., and Knaff, D. B. (2002) *Biochemistry* **41**, 8868–8875
- Osyczka, A., Nagashima, K. V., Sogabe, S., Miki, K., Yoshida, M., Shimada, K., and Matsuura, K. (1998) *Biochemistry* **37**, 11732–11744
- Osyczka, A., Nagashima, K. V., Sogabe, S., Miki, K., Shimada, K., and Matsuura, K. (1999) *Biochemistry* **38**, 15779–15790
- Osyczka, A., Nagashima, K. V., Shimada, K., and Matsuura, K. (1999) *Biochemistry* **38**, 2861–2865
- Knaff, D., Willie, A., Long, J., Kriauciunas, A., Durham, B., and Millett, F. (1991) *Biochemistry* **30**, 1303–1310
- Nagashima, K. V., Shimada, K., and Matsuura, K. (1996) *FEBS Lett.* **385**, 209–213
- Yoshida, M., Masuda, S., Nagashima, K. V. P., Shimada, K., and Matsuura, K. (1998) in *Photosynthesis: Mechanisms and Effects* (Garab, G., ed) Vol. II, pp. 897–900, Kluwer Academic Publishers, Dordrecht, The Netherlands
- Nagashima, K. V. P., Matsuura, K., Wakao, N., Hiraishi, A., and Shimada, K. (1997) *Plant Cell Physiol.* **38**, 1249–1258
- Nagashima, K. V., Sakuragi, Y., Shimada, K., and Matsuura, K. (1998) *Photosynth. Res.* **55**, 349–355
- Béal, D., Rappaport, F., and Joliot, P. (1999) *Rev. Sci. Instrum.* **70**, 202–207
- Chen, S. W., and Pellequer, J. L. (2004) *Curr. Med. Chem.* **11**, 595–605
- Roussel, A., and Cambillau, C. (1989) *Silicon Graphics Geometry Partners Directory*, pp. 77–78, Silicon Graphics, Mountain View, CA
- McRee, D. E. (1992) *J. Mol. Graph.* **10**, 44–47
- Brünger, A. T. (1992) *X-PLOR, Version 3.1. A System for X-ray Crystallography and NMR*, Yale University Press, New Haven, CT
- MacKerell, A. D., Bashford, D., Bellott, M., Dunbrack, R. L., Jr., Evanseck, J. D., Field, M. J., Fisher, S., Gao, J., Guo, H., Ha, S., Joseph-McCarthy, D., Kuchnir, L., Kuczera, K., Lau, F. T. K., Mattos, C., Michnick, S., Ngo, T., Nguyen, D. T., Prodhom, B., Reiher, W. E., III, Roux, B., Schlenker, M., Smith, J. C., Stote, R., Straub, J., Watanabe, M., Wiorkiewicz-Kuczera, J., Yin, D., and Karplus, M. (1998) *J. Phys. Chem. B* **102**, 3586–3616
- Deisenhofer, J., Epp, O., Sinning, I., and Michel, H. (1995) *J. Mol. Biol.* **246**, 429–457
- Matsuura, Y., Takano, T., and Dickerson, R. (1982) *J. Mol. Biol.* **156**, 389–409
- Gonzalez, A., Benini, S., and Ciurli, S. (2003) *Acta Crystallogr. Sect. D Biol. Crystallogr.* **59**, 1582–1588
- Sanner, M. F., Olson, A. J., and Spehner, J.-C. (1996) *Biopolymers* **38**, 305–320
- Strickland, S., Palmer, G., and Massey, V. (1975) *J. Biol. Chem.* **250**, 4048–4052
- Laskowski, R. A., MacArthur, M. W., Moss, D. S., and Thornton, J. M. (1993) *J. Appl. Crystallogr.* **26**, 283–291
- Venturoli, G., Mamedov, M. D., Mansy, S. S., Musiani, F., Strocchi, M., Francia, F., Semenov, A. Y., Cowan, J. A., and Ciurli, S. (2004) *Biochemistry* **43**, 437–445
- Axelrod, H. L., Abresch, E. C., Okamura, M. Y., Yeh, A. P., Rees, D. C., and Feher, G. (2002) *J. Mol. Biol.* **319**, 501–515
- Pelletier, H., and Kraut, J. (1992) *Science* **258**, 1748–1755
- Moser, C. C., Keske, J. M., Warncke, K., Farid, R. S., and Dutton, P. L. (1992) *Nature* **355**, 796–802
- Page, C. C., Moser, C. C., Chen, X., and Dutton, P. L. (1999) *Nature* **402**, 47–52
- Nitschke, W., and Dracheva, S. M. (1995) in *Anoxygenic Photosynthetic Bacteria* (Blankenship, R. E., Madigan, M. T., and Bauer, C. E., eds) pp. 775–805, Kluwer Academic Publishers, Dordrecht, The Netherlands
- Kraulis, P. J. (1991) *J. Appl. Crystallogr.* **24**, 946–950
- Merritt, E. A., and Bacon, D. J. (1997) *Methods Enzymol.* **277**, 505–524